Classifying Photonic Topological Phases Using Manifold Learning

Or Yair*[1], Eran Lustig*[2], Ronen Talmon[1], Mordechai Segev[2]
1. *Viterbi faculty of Electrical Engineering, Technion 32000 Haifa, Israel*
2. *Physics Department and Solid State Institute, Technion, 32000 Haifa, Israel*
msegev@tx.technion.ac.il
**O. Yair and E. Lustig contributed equally to this work*

Abstract: We use Manifold Learning to classify topological phases of photonic systems, from an arbitrary set of measurements without any prior knowledge or assumptions.
OCIS codes: (070.7345) Wave propagation; (150.1135) Algorithms

In recent years, there has been an increasing interest in topological phases in physical systems. Topological phases are separated regions in parameter space, characterized by different topological invariants. The interfaces between topological phases exhibit exotic behavior, displaying unidirectional surface currents that are robust against scattering from disorder and imperfections: phenomena known today as the characteristic features of topological insulators [1,2]. Topological insulators have been suggested to have major applications in quantum computing, giving rise to disorder-protected optical systems and spintronic devices, to name just a few. Specifically, in photonic systems, studies show that topological phases are abundant, appearing in many different systems. Examples are waveguide arrays [3], coupled optical resonators [4], and more. In some of these cases, the systems are nonlinear and/or non-Hermitian, and it is extremely hard to know if the system under study is topological or not, especially when carrying out measurements in an experimental system. In some settings, it is possible to determine if the system is topological by testing transport of edge states, but in many cases this is not accessible or not unequivocal. For example, if the propagation distance in the system is too short to determine whether (or not) the transport is topologically protected. To date, examining physical settings and deciding if they are in a non-trivial topological phase is always hard and often inaccessible, even when the model is known. Recent work proposed to use artificial neural networks for identifying topological phases [5]. However, artificial neural networks rely on known topological models as prior knowledge, as manifested in the network training stage. This poses an inherent problem: using known models to discover new ones has major limitations, especially when considering the new and unexplored regimes. Most certainly, many (possibly infinite) physical models can be topological, and are not associated with any topological model known today.

Here, we use diffusion maps [6], a fundamentally different methodology to classify systems according to their topology without any prior knowledge, based solely on arbitrary measurements. Diffusion maps is a known manifold learning methodology. We show that manifold learning reveals the hidden topology in complex systems, and apply it to simulations and experimental data. Automatically distinguishing between topological phases without any prior knowledge relies on the intrinsically different wavefunction structure of the eigenmodes in different topologies.

Manifold learning is a data-driven method for analyzing complicated data sets. Its main assumption is that often data is constrained to lie on or around a low-dimensional manifold. The idea is then to build a low-dimensional embedding of the data, such that it parametrizes the underlying manifold structure.

We begin by demonstrating the method on an archetypical model known as the Haldane model [7], which underlies many topological systems, and can be described by wavefunctions conforming a honeycomb lattice under a non-uniform magnetic field (Fig.1a). The magnetic field breaks time-reversal symmetry. On the Haldane model, which is topological, we introduce detuning between the two underlying sub-lattices of the honeycomb. The detuning breaks parity symmetry. This detuned Haldane model is in a topological phase when the time reversal breaking is dominant over the parity symmetry breaking, and trivial in the opposite case.

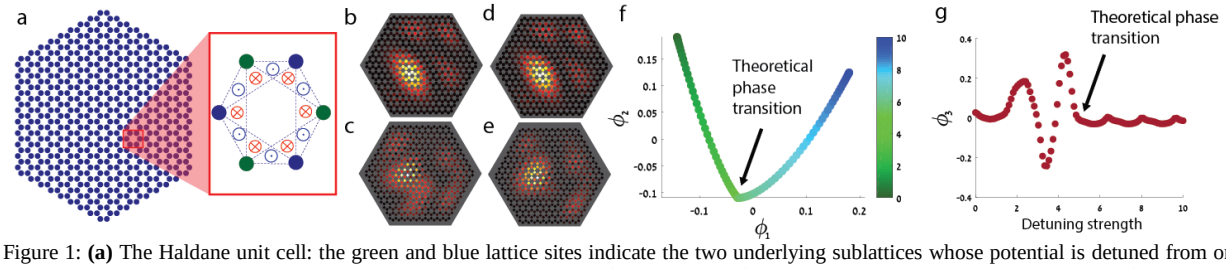

Figure 1: **(a)** The Haldane unit cell: the green and blue lattice sites indicate the two underlying sublattices whose potential is detuned from one another. The red and blue inward and outward arrows are the non-uniform magnetic field. **(b,d)** Arbitrary initial bulk excitation of the Haldane model in the topological and the trivial cases, respectively (low and high detuning). **(c,e)** The state of (b,d) after time KT, respectively. **(f)** Scatter plot of the first two principal components of diffusion maps in the first simulation. The points are colored by the detuning in the honeycomb potential. **(g)** The third principal components of diffusion maps as a function of the detuning in the second simulation.

We use this detuned-Haldane model as a testbed to simulate the ability of manifold learning to classify the topological phases of the system. In the first simulation, we generate random initial wavefunctions for 100 different detuned Haldane systems, each with its detuning, and observe how initial wavefunctions evolve in a system with $M = 157$ sites (Fig.1b-e).

In experimenting with the detuned Haldane system, it is possible to observe whether the system is topological (or not) by examining the dispersion curve (very hard to do in experiments), or by examining the propagation of edge states, which is very demanding and not unequivocal in experiments. We are therefore motivated to simulate the more challenging case where the excitation is only in the bulk and not on the edges (Fig.1b,d). In the propagation simulations we used, there is no visible deference between the phases (Fig.1c,e). However, our manifold learning algorithm is able to make a clear distinction between the phases and classify them correctly. In brief, let $\psi_m^i(t) \in \mathbb{C}$ be the wavefunction, where $m \in \{1,2,\dots,M\}$ is the site, $t \in \{T, 2T, \dots, KT\}$ is time, where KT is larger than the typical dynamics of the system, and $i \in \{0.1,0.2,\dots,10\}$ is the normalized detuned potential. We then apply diffusion maps to $\{\psi^i \in \mathbb{C}^{M\times K}\}_i$ where ψ^i is the evolution of the entire lattice i (with its specific detuning). Diffusion maps provides a new representation to $\{\psi^i\}_i$, taking into account the local relations between the different $\{\psi^i\}_i$ and parametrizing the global manifold structure into a Euclidean space. In Fig.1f, we present the first two "principal components" of diffusion maps. The topological phases are distinguishable in the new representation.

The first simulation relied on monitoring transport of arbitrary excitation. However, examining the full evolution (absolute value and phase) for an extended period, is often not accessible in experiments. Therefore, we repeat the process with a second simulation, which uses as input data that is more accessible experimentally: the amplitude at the final time KT, $\{|\psi_m^i(KT)|\}_i$, and only that. We excite the system as in the first simulation, but in this scenario, we use 200 different random bulk excitations for each detuned Haldane model. First, for each detuned Haldane model we compute the sample covariance from the 200 different random excitations. Then, we apply diffusion maps to the 200 covariance matrices with the Riemannian norm [8]. In Fig.1g we present the third principle component of diffusion maps as a function of the detuning. The phases are still distinguishable. We note they are distinguishable also in the first two components, but we chose to present the third since there, it is pronounced best visually.

Next, we demonstrate the method on recently published experimental results of a photonic type-2 Weyl point [9]. The photonic Weyl point is a band-crossing point in the spectrum of a 3D lattice. Ref. [9] demonstrates how a 2D waveguide array (Fig.2a) can have a Weyl point in its spectrum when considering the wavelength as a third degree of freedom. The Weyl point can be viewed on a phase diagram as a boundary in frequency and lattice-period space (Fig.2b). The experimental data is 145 intensity (amplitude) pictures at the output of the system (Fig.2c), on which we use diffusion maps. In Fig.2d we plot a low dimensional presentation of the diffusion maps principle components using tSNE [10]. Interestingly, the Weyl point is manifested visually as a 'knee' point in the new representation. Arranging all points on a wavelength – lattice-period space gives the reconstructed phase diagram which is just slightly different than the theoretical one (Fig.2e). These differences are within the experimental margins of error.

To conclude, we introduced a manifold learning approach for identifying topological phases based on partial arbitrary information without any prior knowledge or assumptions.

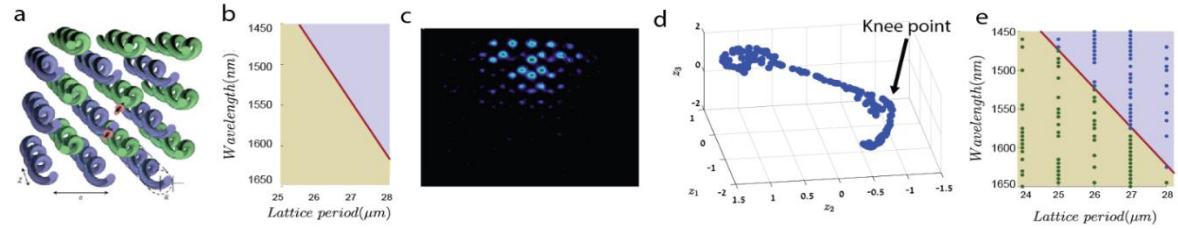

Figure 2: **(a)** Helical waveguide array of the experiment of [13]. **(b).** Calculated phase diagram related to the Weyl point (red line) in the system of (a) **(c)** Example of an experimental output intensity image. **(d)** A dimensionality reduction (tSNE) presentation to the obtained reparameterization (diffusion maps) to the real experimental Weyl data.**(e)** Extracted phase diagram. Each point corresponds to an experiment. The color of each point is based on its position relative to the break point of the curve in (c). Green points are to the left of the break point, and blue to the right.

[1] C. L. Kane and E. J. Mele, Phys. Rev. Lett. 95, 226801 (2005).
[2] B. A. Bernevig, T. L. Hughes, and S. C. Zhang, Science 314, 1757 (2006).
[3] M. C. Rechtsman et al, Photonic Floquet Topological Insulators, Nature (London) 496, 196 (2013).
[4] M. Hafezi, S. Mittal, J. Fan, A. Migdall, and J. M. Taylor, Imaging Topological Edge States in Silicon Photonics, Nat. Photo. 7, 1001 (2013).
[5] Evert P. L. van Nieuwenburg, Ye-Hua Liu and Sebastian D. Huber, Nature Physics 13, 435–439 (2017)
[6] R. R. Coifman and S. Lafon, Diffusion maps, Appl. Comput. Harmon. Anal., vol. 21, no. 1, pp. 530, 2006.
[7] F. D. M Haldane, Phys. Rev. Lett. 61, 2015 (1988)
[8] Pennec, X., Fillard, P., and Ayache, N. 2005. A Riemannian framework for tensor computing. International J. Computer Vision, 65(1).
[9] J. Noh, S. Huang, D. Leykam, Y. D. Chong, K. P. Chen and M. C. Rechtsman, Nature Physics 13, 611–617 (2017)
[10] L. van der Maaten and G. E. Hinton, "Visualizing data using t-Sne," Journal of Machine Learning Research, vol. 9, 2579, November 2008.